

Effect of Particle Size on Optical Properties of Powder Bed with Near-Infrared Laser for Large Scale Powder Bed Fusion Process in Polymer

Yuki Yamauchi, Koichi Fujii, Takashi Kigure, Yuki Asano

Tokyo Metropolitan Industrial Technology Research Institute, 2-4-10 Aomi Koto-ku, Tokyo,
Japan

Abstract

Given the potential for expanding applications of polymer powder bed fusion in the automotive and aerospace industries, developing an efficient, large-scale process with high productivity is required. To increase the productivity of polymer powder bed fusion, it's important to process larger areas in a short period. This process focuses on the optical properties of the powder bed, such as the penetration depth of the incident laser or its reflection, to increase the melting depth in a single-layer process. Previous studies have suggested that although the use of a near-infrared laser is effective in increasing the penetration depth, most of the laser energy is lost through diffuse reflection. In this study, the authors attempted to reduce the particle interface by increasing the particle size and confirmed that this reduced the diffuse reflection and increased the penetration depth. In addition, the melting depth was increased by using larger powder sizes with the same laser energy.

Introduction

Additive manufacturing (AM) technologies have recently been scaled up not only in the construction industry but also in sectors such as the automotive and aviation industries. For example, material extrusion using polymers can produce meter-scale parts with robotic arms or frame structures that are as large as an entire room[1]. This is no exception for polymer powder bed fusion (PBF-P), which is one of the most promising AM technologies for producing end-use parts. Currently, some of the largest PBF-P machines offer build volumes of up to 1000 mm × 540 mm × 400 mm, with expectations of even larger capacities in the future[2]. However, the layering pitch or height per layer in PBF-P remained relatively unchanged. Consequently, fabricating large parts, especially those several meters tall, requires the deposition of thousands of layers. Although the speed of layer fabrication has improved in some respects[3][4], the overall build time for large parts remains substantial. Increasing the layer height is a key strategy to improve building efficiency[5][6]. However, this approach introduces challenges such as weak or incomplete bonding between layers[7]. To ensure sufficient bonding, the fusion depth must exceed the thickness of the powder layer. This can be achieved by increasing the input energy from the light source, for example, by increasing the laser power[8].

Another critical factor is the penetration depth of the light source into the powder bed[9]. CO₂ lasers, which are commonly used in PBF-P systems[10], have limited penetration owing to the high absorption of most polymers[11]. If the laser power is increased without improving the penetration depth, most of the energy will be absorbed near the surface, causing excessive heating and potential thermal degradation of the polymer. Meanwhile, the deeper regions of the

powder bed remain insufficiently heated. To address this issue, alternative methods have been proposed to enhance the penetration depth, such as using near-infrared (NIR) lasers, which are less readily absorbed by polymers[12]. For example, previous research by the author demonstrated that NIR light can penetrate a polymer powder bed to depths more than five times greater than CO₂ lasers[13]. The penetration depth can be tuned by adding an absorbent to the powder. However, NIR light tends to undergo significant diffuse reflection, particularly when the absorbent concentration is low (Fig. 1). This reflection results in energy loss and reduces heating efficiency, limiting the penetration depth.

Therefore, a novel process is required to reduce diffuse reflection and enhance penetration depth, particularly for large powder beds and large-scale PBF applications. This study focuses on the role of particle boundary faces in the powder layer, which significantly influences diffuse reflection in NIR-based PBF-P. The boundary surface area was controlled by adjusting the particle size, and the optical properties of the powders with various particle sizes were examined. This study also investigated the effect of particle size on the depth of fusion.

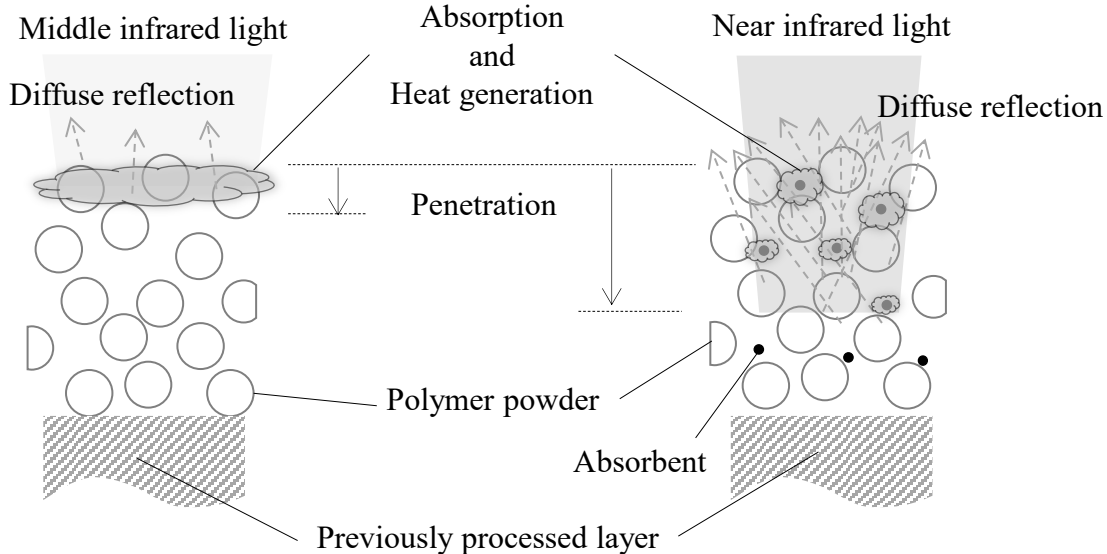


Figure 1: Differences in diffuse reflection and penetration of the incident light for each light source in the previous PBF-P. The left shows the case of middle infrared light, and the right shows the case of near infrared light.

Material and Methods

Preparation of powder material with various particle sizes

This study involved three steps for obtaining polymer powders with various particle sizes. First, relatively small pellets (approximately 0.5 mm) were prepared using a pelletizer with commercially available polymer powder (ASPEX-PA12Neo with an average diameter of 60 μm from Aspect, Inc., Japan). The process was performed by a material processing company (Gurantsu Corporation, Japan). Second, the prepared pellets were turned into a powder by cryo-crushing with liquid nitrogen, which was also performed by another material processing company (OSAKA GAS LIQUID Co., Ltd., Japan). Lastly, the crushed powder was separated using a sieve with openings of 150, 250, and 500 μm.

To enhance the absorption of near-infrared (NIR) light and generate heat for powder melting, colorant powder (Nubian Black PC-0870, Orient Chemical Industries Co., Ltd.) was added to the prepared powder to evaluate the depth of fusion, as described below. The absorbent content was 0.2 wt% for each prepared powder.

Evaluation of Prepared Powders

In addition to measuring the optical properties of each powder, we evaluated its particle size distribution, morphology, and thermal properties. A simple device equipped with a microscope and image processing software (Portable Pita, SEISHIN ENTERPRISE Co.,Ltd., Japan) was used for preliminary analysis of the particle size distribution. Benchtop scanning electron microscope was used to observe the particle shapes. A differential scanning calorimeter (DSC8230, Rigaku, Japan) was used for thermal analysis to calculate the melting point and heat of fusion from the obtained DSC curve. Transmittance and diffuse reflectance were measured for various powder layer thicknesses using a method described in the literature [13]. An integrated sphere coated with BaSO₄ was used to measure diffuse reflectance. Given the sphere throughput, the diffuse reflectance was calculated relative to a standard specimen for which the reflectance was known. Transmittance was obtained by calculating the ratio of input energy to transmitted energy using a laser power sensor (L50(150)A-BB-35, Ophir Optronics Solutions Ltd.), accounting for energy loss through the SiO₂ window. The penetration depths D_p were obtained from the relationship between the powder layer thickness z and the transmittance T , based on the Beer–Lambert law, as shown in Equation 1.

$$T = e^{-\frac{z}{D_p}} \quad (1)$$

Single layer fabrication

The depth of fusion was obtained using the prepared powder (D50 = 450 μm) and the commercially available powder was used as a control based on the thickness of the single-layer fabricated region. For this experiment, a commercially available PBF-P machine (RaFaEl 300F, Aspect Inc., Japan) equipped with a 1 μm NIR fiber laser was used. In this experiment, the laser beam diameter was 170 μm at the powder bed. The experimental conditions, including laser power, are listed in Table 1. Although the powder bed is typically heated between the recrystallization temperature and melting point in the PBF-P process, the powder bed was not heated for this brief test. The input energy of the laser was chosen based on the energy required for melting, which was calculated from parameters such as the heat of fusion and specific heat; this value was the same for each powder. A spherical micrometer was used to measure its thickness. Additionally, cross sections of the fabricated specimens were observed using epoxy embedding to analyze the melting state of each powder.

Table 1: Experimental conditions

Bed Temperature °C	30
Scan speed m/s	0.5
Scan spacing mm	80
Laser power W	30
Scan area mm	10×10

FEM Transient Heat Transfer Analysis

As described below, the thermal properties of the prepared powders changed because of remelting and rapid cooling during palletization. These properties can affect the temperature during fabrication or in the melting region. To properly discuss the effect of the optical properties of the powders, the depth of fusion was calculated through finite element modeling (FEM) analysis with transient heat transfer based on various thermal properties. This analysis was based on a rough estimation described in our previous report[14]. In this estimation, the heat generation was calculated based on the penetration depth and input energy. The thermal properties of each powder for this analysis are listed in Table 2, and Prepared powder of each property is based on the experimental results of this study. Control powder of each property was obtained from material supplier. Although the heat of fusion was the thermal dependence obtained from the DSC curve, it was assumed that the specific heat was constant for all powders as $2.65 \text{ J/g} \cdot \text{K}$. The laser power, scan speed, and scan spacing are the same as those listed in Table 1. In addition, the analysis also considered powders whose thermal properties do not change after particle size adjustment (Supposition). Which means that the Supposition prepared powder has the same properties as the control.

Table 2: Thermal properties of each powder

Powder	Prepared, $D_{50} = 450 \text{ } \mu\text{m}$	Control
Heat of fusion J/g	48.6	90.0
Melting point $^{\circ}\text{C}$	178	189

Results and Discussion

Particle Size Adjustments

Figure 2 shows the particle size distribution of the prepared powders. The median diameters of the powders were 250, 450, and 650 μm . Given that the median diameter of the control powder (commercially available) is 60 μm , it is evident that powders of various sizes and sufficiently larger diameters have been successfully prepared.

Figure 3 shows scanning electron microscope (SEM) images of the powders. The particle sizes of the powders were different, which supported the particle size distribution results. Interestingly, the morphologies of the powders differed. The large powder particles were spherical, whereas the small powder particles had high aspect ratios. The large powder did not undergo as much crushing as the small powder; it may have simply been rounded owing to the impact of the crushing process. These results may have been affected by the cryo-crushing parameters and further investigation is required.

Figure 4 shows the differential scanning calorimetry (DSC) curves of each powder. Compared to the control powder, the prepared powders had lower melting points and heats of fusion. The reasons for this are discussed below: Most commercially available PBF powders are produced using a precipitation method[15], which results in high crystallinity. Conversely, pelletized polymers exhibit relatively low crystallinity owing to the rapid cooling during extrusion. In this study, the powder was prepared via pelletizing and cryo-crushing, resulting in a low crystallinity, low melting point, and low heat of fusion.

Figure 5 (a) illustrates the relationship between the powder layer thickness and diffuse reflection. As the thickness of the powder layer increased, the diffuse reflection tended to increase for all powders. At the same thickness, larger powders exhibited lower diffuse reflection. Although the crystallinity of the powder, as mentioned above, may affect diffuse reflection, the prepared powder showed a significantly lower reflection than the control powder. Figure 5 (b) shows the relationship between the thickness of the powder layer and transmittance. As expected, the transmittance decreased as the thickness of the powder layer increased. The larger powders maintained a high transmittance even when the powder layer became thicker. In addition, the penetration depth is greater for larger particles, as shown in Figure 6. These results suggest that reducing the boundary face reduces the diffuse reflection and allows light energy to penetrate deeper.

Figure 7 shows the measured optical properties of the prepared powder ($D_{50} = 450 \mu\text{m}$) and the control powder containing the absorbent. As expected, the diffuse reflectance and transmittance decreased with the addition of the absorbent. However, the effect of adjusting the particle size is clear. The penetration depth of the prepared powder with the absorbent was greater than that of the control powder without the absorbent, as shown in Figure 8. Thus, this method allows us to deliver light energy to deeper regions while ensuring heat generation.

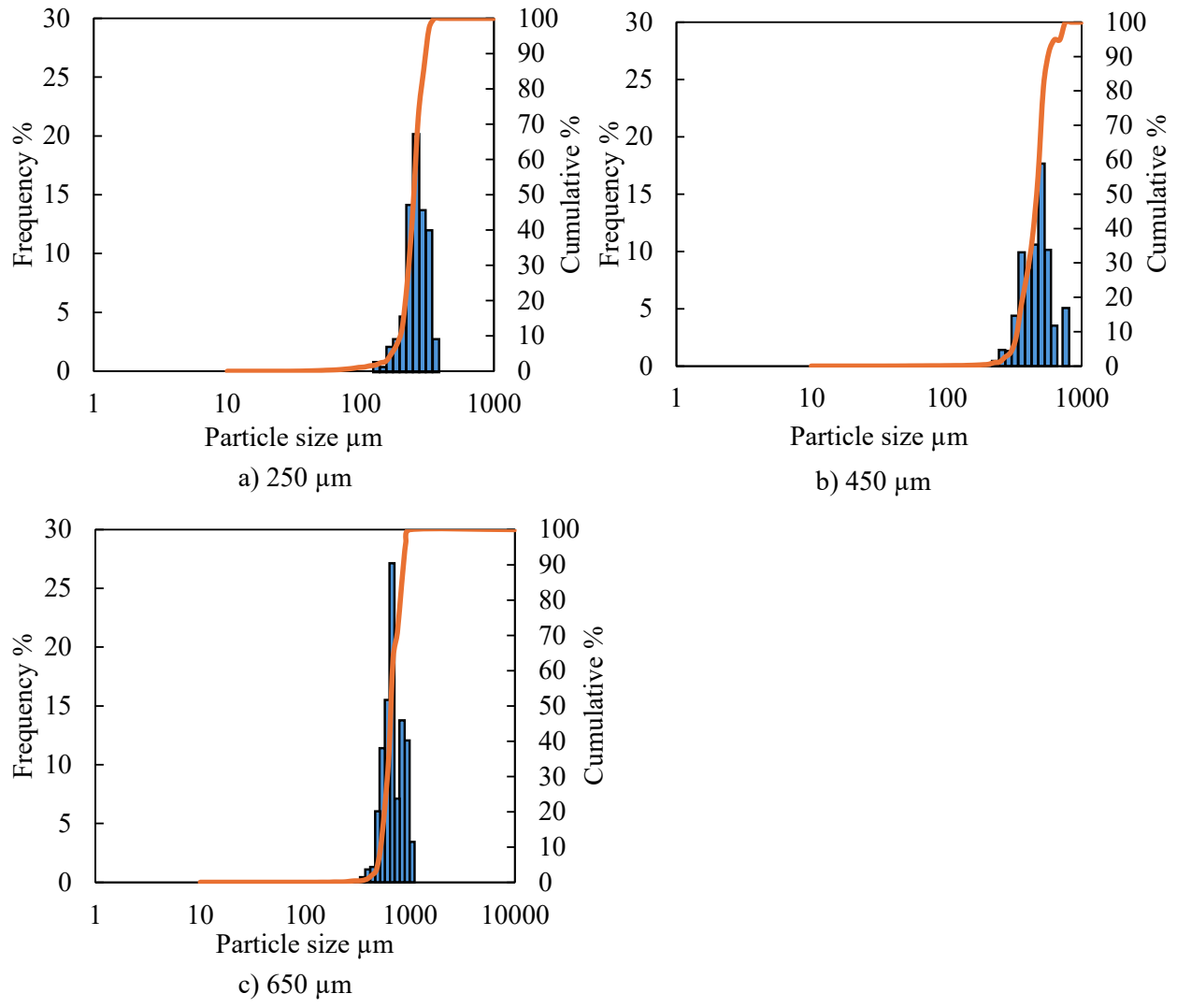
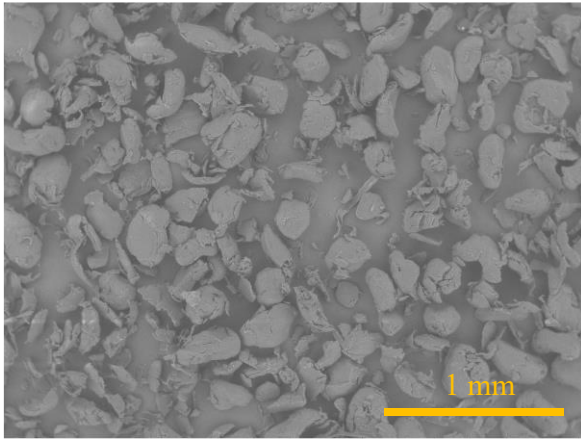
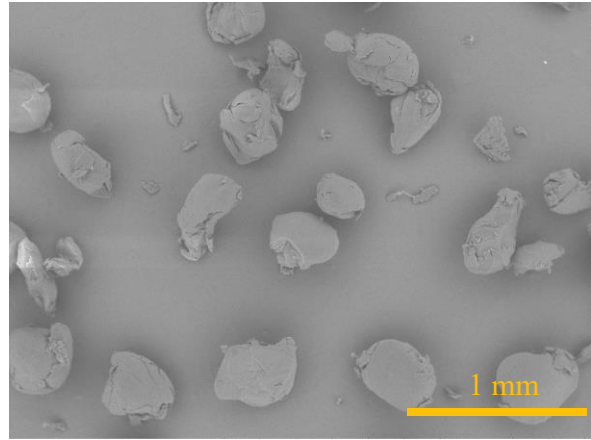


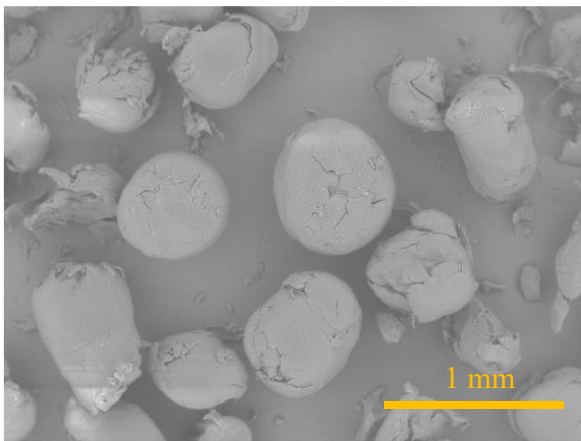
Figure 2: Particle distribution for each powder



a) 250 μm



b) 450 μm



c) 650 μm

Figure 3: SEM images of each powder

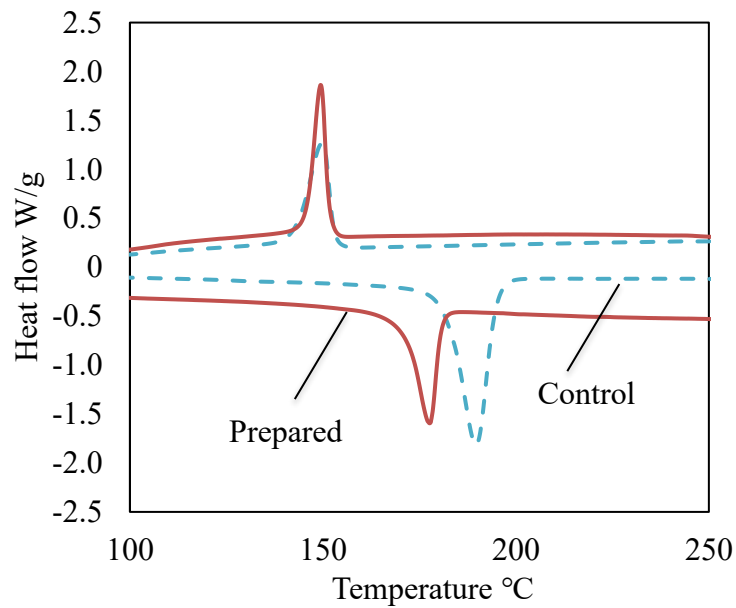


Figure 4: DSC curves of prepared and control powder

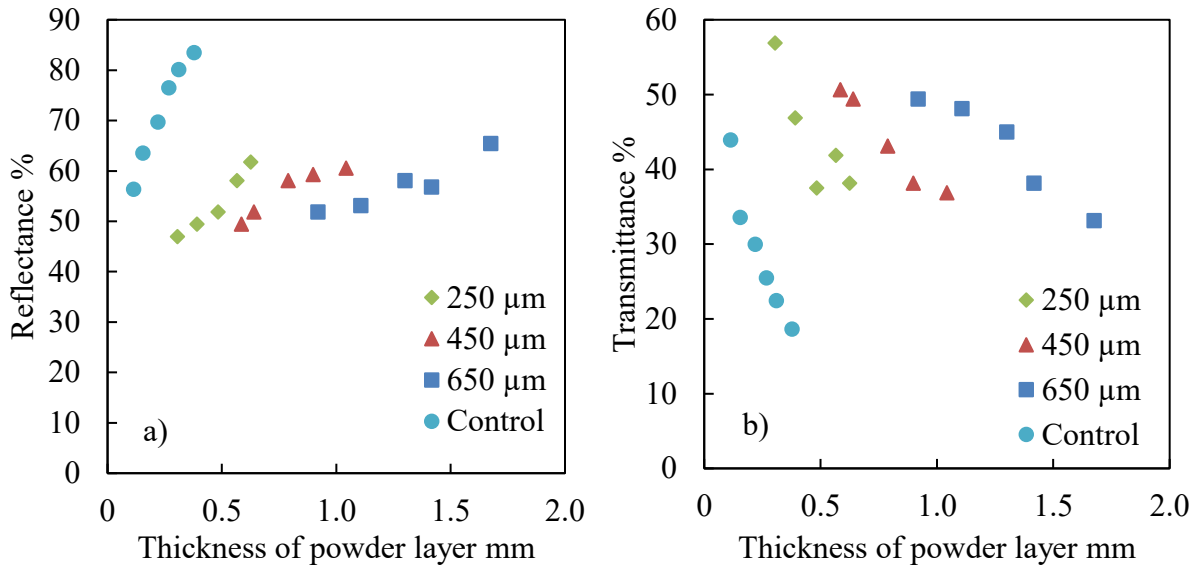


Figure 5: Optical properties of each powder

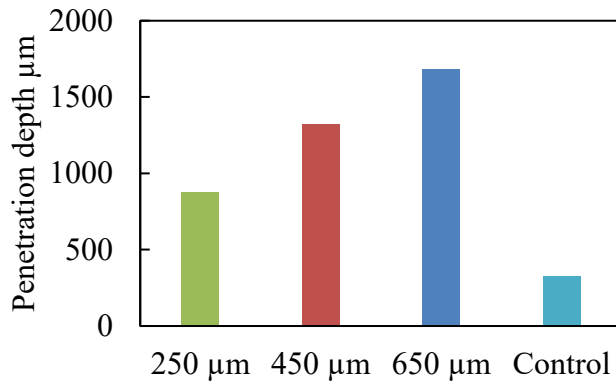


Figure 6: Penetration depth of each powder

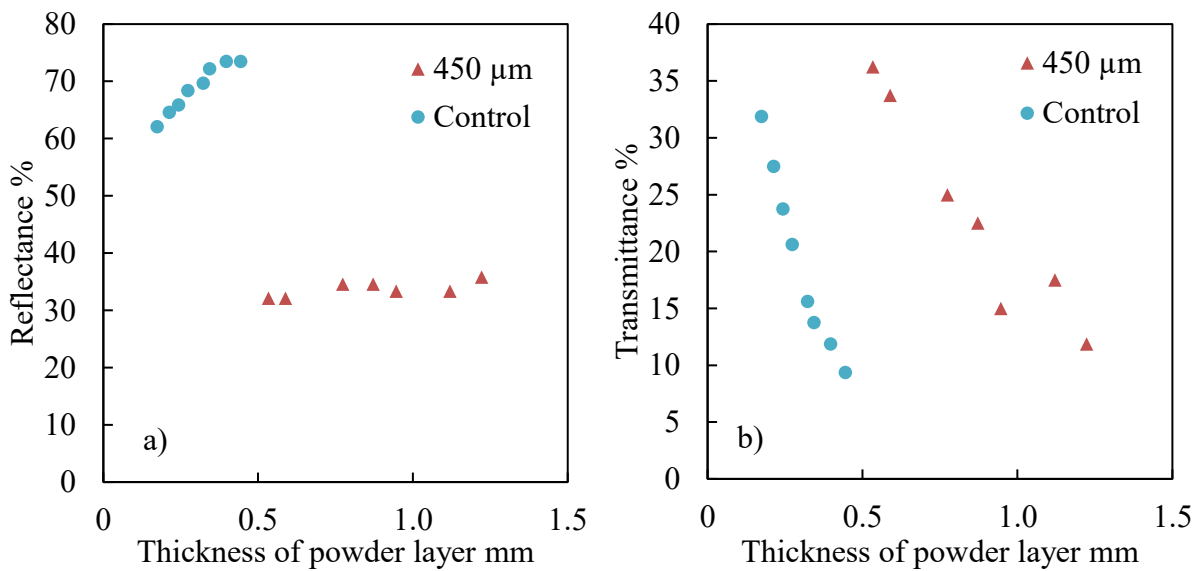


Figure 7: Optical properties of powders with absorbent

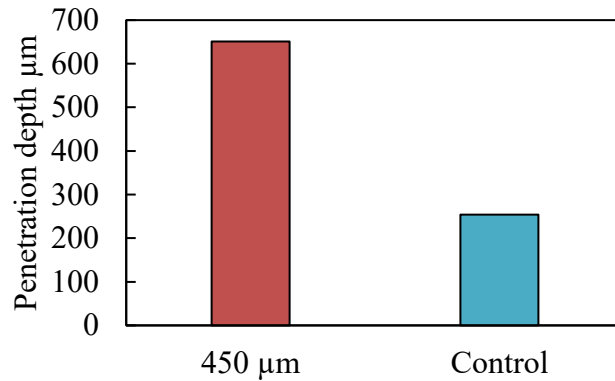


Figure 8: Penetration depth of powders with absorbent

Single Layer Fabrication

Figure 9 shows photographs of the specimens obtained from single-layer fabrication. As previously mentioned, because the powder bed was not heated and no anchors were set, the region melted by the laser irradiation solidified and shrank rapidly[16]. Consequently, drastic aggregation occurred, particularly in the melt region, as shown in the figure. The cross-sectional images of the specimens are shown in Figure 10. It seemed that the particles in the prepared powder did not melt completely. The reasons for this are discussed below: Naturally, the dry-blended absorbents were placed around the polymer particles and not within them. In this case, the absorbents become much more segregated with larger particles, indicating that there is a greater distance between the centers of the particles and absorbents. This makes it difficult for the absorbents to transfer heat to the center of the polymer particles. Consequently, only the surfaces of the polymer particles melted. Additionally, the volume of voids between the particles increases as the particle size increases. The molten polymer must flow well to fill the voids. In fact, there is nearly no flow in the deep regions of the powder layer, where the energy decays. Large voids remain, as shown in Figure 11. Therefore, to melt the large particles, it is important to disperse the absorbent in the powder bed. An effective way to disperse the absorbent is through melt-kneading.

Figure 12 shows the thickness of the specimens obtained via single-layer fabrication. The specimen from prepared powder was thicker than the control specimen. This could be due to a low diffuse reflection and a large penetration depth, which was achieved by reducing the boundary face of the powder layer through particle size adjustment. However, the decrease in melting point and heat of fusion may have affected the thickness of the specimens prepared from the powder. Conversely, specimens from the control powder may have had varying thicknesses due to agglomeration, or in other words, may have been thicker than expected due to agglomeration.

FEM Transient Heat Transfer Analysis

Figure 13 shows the distribution of maximum temperatures for each element obtained from the FEM analysis. The temperatures at the surface and in the deeper regions of the prepared powder were higher than those of the control powder, although the input energy and absorbent content were the same. These results must be due to less light energy loss from diffuse reflection and greater penetration depth. The depth of the melt region for each powder, as obtained from FEM analysis, is shown in Figure 14. The calculated depth was similar to the depth of fusion

obtained through single-layer fabrication. However, the calculated depth is smaller than that obtained experimentally. As the experimental results show, although aggregation is quite strong in the control powder, this calculation does not consider the mass flow. It is assumed that the single-layer region fabricated from the control powder becomes thicker owing to aggregation. Further investigations are required to understand the influence of aggregation on the depth of fusion obtained from the experiment, or the difference between the calculated and experimental depths.

Regarding the melting temperature or heat of the fusion drop in the prepared powder, the calculation results showed that the effect of reducing the boundary face on the depth of fusion was negligible. Therefore, reducing the diffuse reflection and increasing the penetration depth were the dominant factors affecting the depth of fusion.

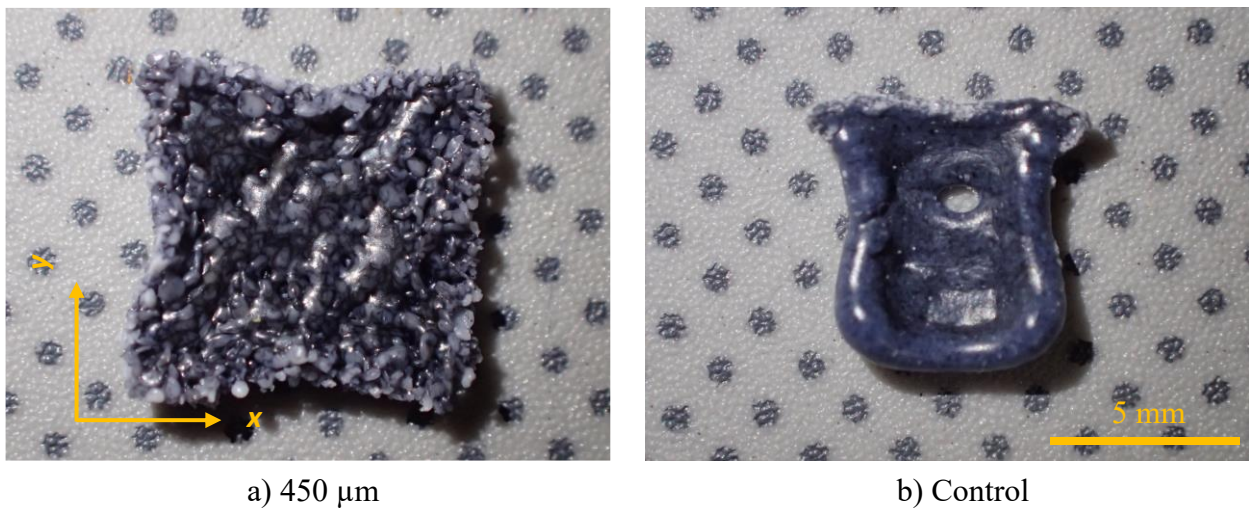


Figure 9: Photos of fabricated specimens. The laser scan direction is along the x -axis, and the travel direction is along the y -axis.

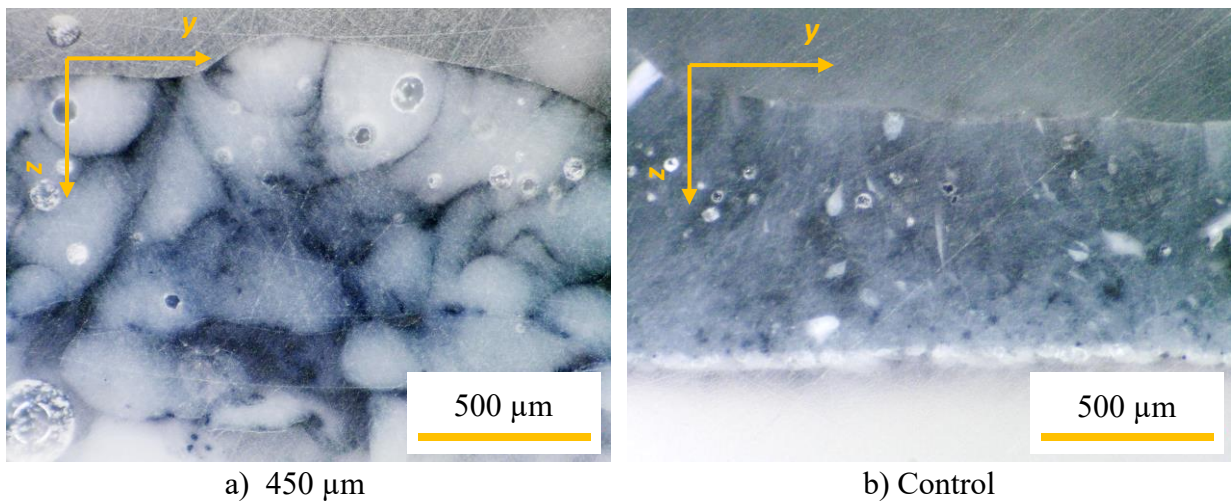


Figure 10: Cross sectional images of fabricated specimens

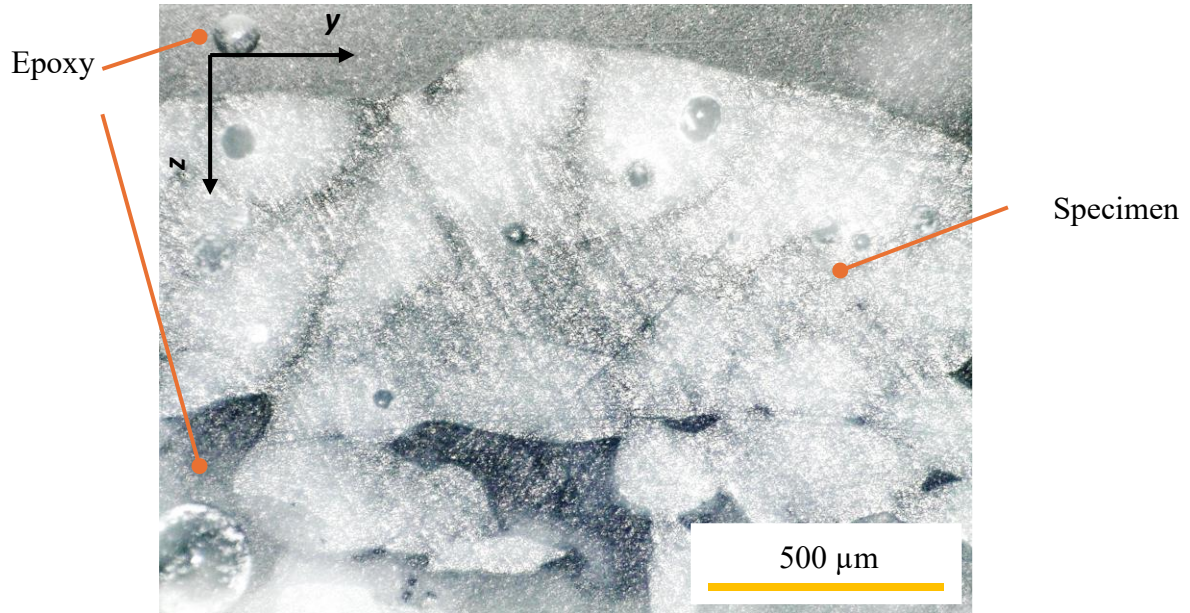


Figure 11: Cross sectional image of fabricated specimen from prepared powder

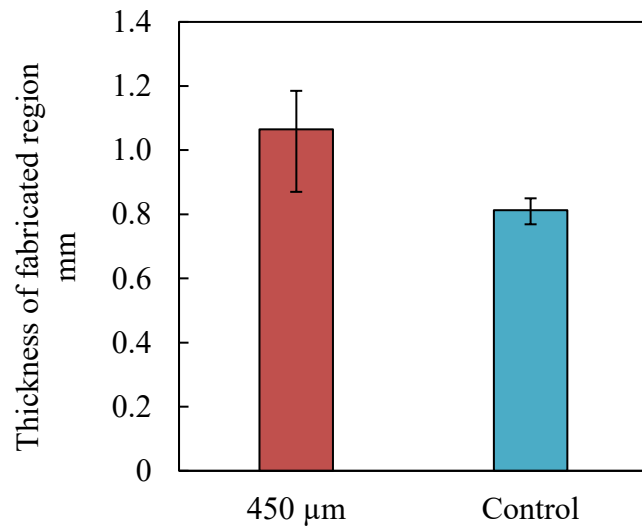


Figure 12: Thickness of fabricated specimens

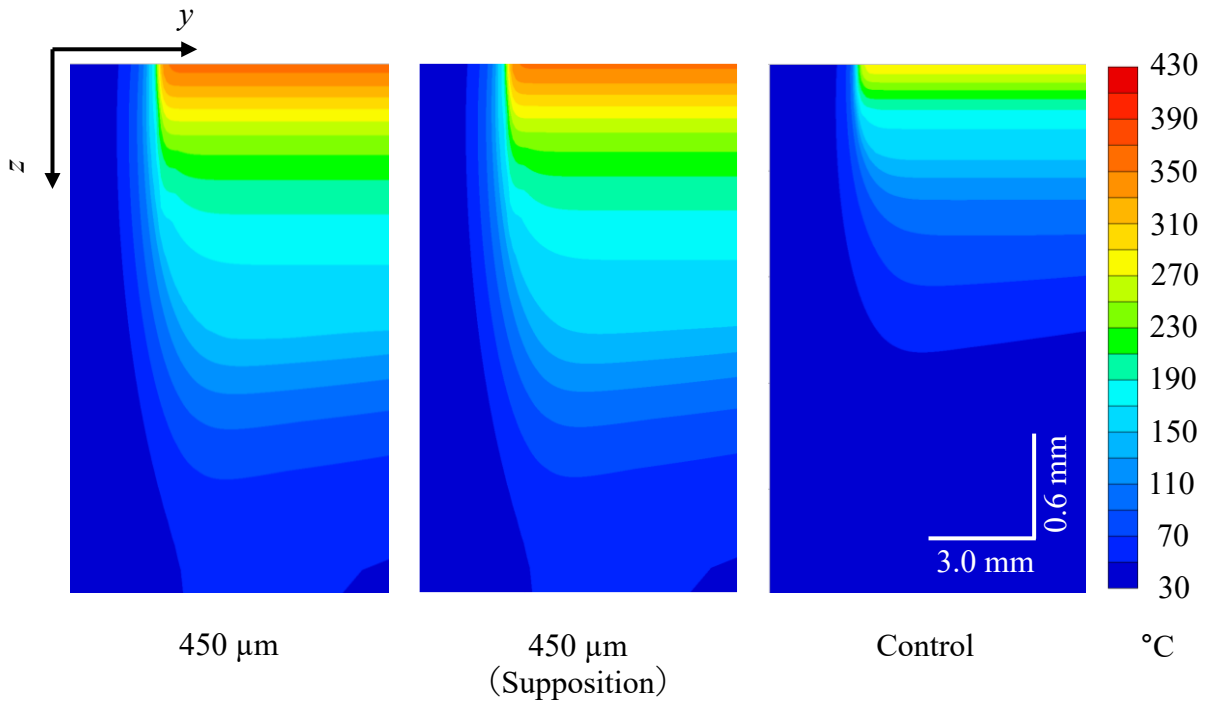


Figure 13: Temperature distribution from FEM analysis

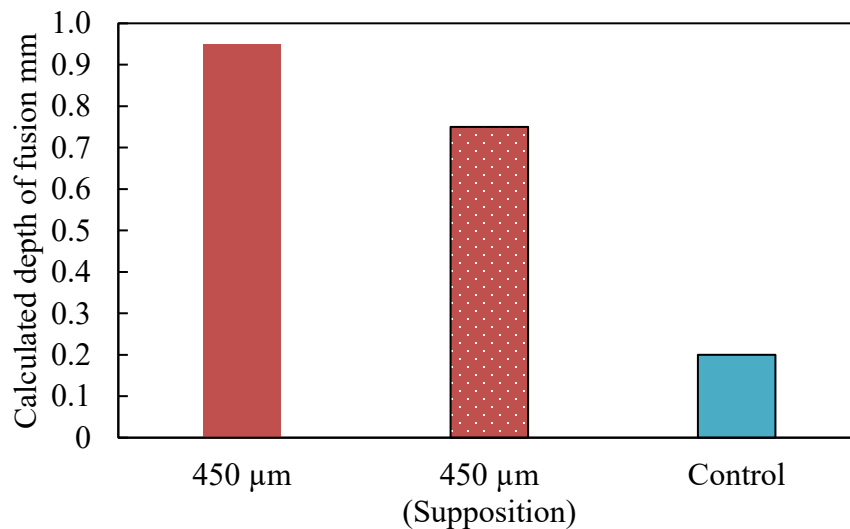


Figure 14: Calculated depth of melting region

Conclusion

This study focuses on reducing the boundary face of the powder layer to improve energy efficiency using an NIR laser, which is rarely absorbed by the polymer, as a light source and on increasing the fabrication region in PBF-P. First, powders of various sizes were prepared via pelletization, cryo-crushing, and sieving. The properties of the prepared powders were then measured. Additionally, the effect of particle size on the energy efficiency was evaluated using the prepared powders through single-layer fabrication and FEM analysis. The following

conclusions were drawn from these investigations: As the particle size increased, the diffuse reflection of the incident NIR laser on the polymer powder layer decreased and the penetration depth increased. Despite the addition of an absorbent to generate heat with an NIR light source, the penetration depth of the large-particle powders was higher than that of commercially available PBF powders without an absorbent. Larger particle powders achieve a greater depth of fusion, even when the same amount of energy is input by the light source. This tendency was also evident in the FEM analysis and supported the conclusions of this study.

Acknowledgment

This work was supported by JSPS KAKENHI (grant number 23K03615). We would like to thank Editage (www.editage.jp) for English language editing.

References

- [1] “Robotic Arm (LFAM)” [Online]. Available: <https://www.proto21.ae/robotic-arm>.
- [2] “VX1000 HSS” [Online]. Available: <https://www.voxeljet.com/industrial-3d-printer/serial-production/vx1000-hss/>.
- [3] Majewski, C. E., Oduye, D., Thomas, H. R., and Hopkinson, N., 2008, “Effect of Infra-Red Power Level on the Sintering Behaviour in the High Speed Sintering Process,” *Rapid Prototyp. J.*, **14**(3), pp. 155–160.
- [4] Ellis, A., Brown, R., and Hopkinson, N., 2015, “The Effect of Build Orientation and Surface Modification on Mechanical Properties of High Speed Sintered Parts,” *Surf. Topogr. Metrol. Prop.*, **3**(3).
- [5] Matilainen, V., Piili, H., Salminen, A., Syvänen, T., and Nyrrhilä, O., 2014, “Characterization of Process Efficiency Improvement in Laser Additive Manufacturing,” *Phys. Procedia*, **56**(C), pp. 317–326.
- [6] Leicht, A., Fischer, M., Klement, U., Nyborg, L., and Hryha, E., 2021, “Increasing the Productivity of Laser Powder Bed Fusion for Stainless Steel 316L through Increased Layer Thickness,” *J. Mater. Eng. Perform.*, **30**(1), pp. 575–584.
- [7] Han, W., Kong, L., and Xu, M., 2022, “Advances in Selective Laser Sintering of Polymers,” *Int. J. Extrem. Manuf.*, **4**(4).
- [8] Yehia, H. M., Hamada, A., Sebaey, T. A., and Abd-Elaziem, W., 2024, “Selective Laser Sintering of Polymers: Process Parameters, Machine Learning Approaches, and Future Directions,” *J. Manuf. Mater. Process.*, **8**(5), p. 197.
- [9] Bourell, D., Coholich, J., Chalancon, A., and Bhat, A., 2017, “Evaluation of Energy Density Measures and Validation for Powder Bed Fusion of Polyamide,” *CIRP Ann. - Manuf. Technol.*, **66**(1), pp. 217–220.
- [10] Bourell, D. L., Watt, T. J., Leigh, D. K., and Fulcher, B., 2014, “Performance Limitations in Polymer Laser Sintering,” *Phys. Procedia*, **56**(C), pp. 147–156.
- [11] Schuffenhauer, T., Stichel, T., and Schmidt, M., 2020, “Experimental Determination of Scattering Processes in the Interaction of Laser Radiation with Polyamide 12 Powder,” *Procedia CIRP*, **94**, pp. 85–88.
- [12] Kroh, M., and Eyerer, P., 2010, “Additive Assisted Laser Sintering of Polyetheretherketone : Influence of Process Parameters and Additives on Morphology Development,” *Proc. Polym. Process. Soc. 26th Annu. Meet.*

- [13] Yamauchi, Y., Kigure, T., Isoda, K., and Niino, T., 2021, “Powder Bed Penetration Depth Control in Laser Sintering and Effect on Depth of Fusion,” *Addit. Manuf.*, **46**(July), p. 102219.
- [14] Kigure, T., Yamauchi, Y., and Niino, T., 2022, “Investigation into Effect of Beam Defocusing in Low Temperature Laser Sintering of PEEK,” *Proc. 33rd Annu. Int. Solid Free. Fabr. Symp. – An Addit. Manuf. Conf.*, pp. 2271–2281.
- [15] Schmid, M., 2018, *Laser Sintering with Plastics: Technology, Processes, and Materials*, Kluwer Academic Publishers.
- [16] Niino, T., Haraguchi, H., Itagaki, Y., Iguchi, S., and Hagiwara, M., 2011, “Feasibility Study on Plastic Laser Sintering without Powder Bed Preheating,” *2011 Int. Solid Free. Fabr. Symp.*, pp. 17–29.